CrossMark

Investigating particle acceleration dynamics in interpenetrating magnetized collisionless super-critical shocks

W. Yao [1,2],†, **A. Fazzini**[1], **S.N. Chen**[3], **K. Burdonov**[1,2,4], **J. Béard**[5],
M. Borghesi[6], **A. Ciardi**[2], **M. Miceli** [7,8], **S. Orlando**[8], **X. Ribeyre**[9],
E. d'Humières[9] **and J. Fuchs**[1]

[1]LULI – CNRS, CEA, UPMC Univ Paris 06 : Sorbonne Université, Ecole Polytechnique, Institut Polytechnique de Paris, F-91128, Palaiseau cedex, France

[2]Sorbonne Université, Observatoire de Paris, Université PSL, CNRS, LERMA, F-75005 Paris, France

[3]'Horia Hulubei' National Institute for Physics and Nuclear Engineering, RO-077125 Bucharest-Magurele, Romania

[4]JIHT, Russian Academy of Sciences, 125412 Moscow, Russia

[5]LNCMI-T, CNRS, Toulouse, France

[6]Centre for Plasma Physics, The Queen's University of Belfast, University Road, BT71NN Belfast, UK

[7]Dipartimento di Fisica e Chimica E. Segrè, Università degli Studi di Palermo, 90134 Palermo, Italy

[8]INAF, Osservatorio Astronomico di Palermo, 90134 Palermo, Italy

[9]University of Bordeaux, Centre Lasers Intenses et Applications, CNRS, CEA, UMR 5107, F-33405 Talence, France

Colliding collisionless shocks appear in a great variety of astrophysical phenomena and are thought to be possible sources of particle acceleration in the Universe. We have previously investigated particle acceleration induced by single super-critical shocks (whose magnetosonic Mach number is higher than the critical value of 2.7) (Yao *et al.*, *Nat. Phys.*, vol. 17, issue 10, 2021, pp. 1177–1182; Yao *et al.*, *Matter Radiat. Extrem.*, vol. 7, issue 1, 2022, 014402), as well as the collision of two sub-critical shocks (Fazzini *et al.*, *Astron. Astrophys.*, vol. 665, 2022, A87). Here, we propose to make measurements of accelerated particles from interpenetrating super-critical shocks to observe the 'phase-locking effect' (Fazzini *et al.*, *Astron. Astrophys.*, vol. 665, 2022, A87) from such an event. This effect is predicted to significantly boost the energy spectrum of the energized ions compared with a single super-critical collisionless shock. We thus anticipate that the results obtained in the proposed experiment could have a significant impact on our understanding of one type of primary source (acceleration of thermal ions as opposed to secondary acceleration mechanisms of already energetic ions) of ion energization of particles in the Universe.

Key words: plasma nonlinear phenomena, plasma simulation

† Email address for correspondence: yao.weipeng@polytechnique.edu

1. Introduction

The particular origins of the high-energy particles (cosmic rays) flying through the Universe is still an open question. We know where they can possibly originate (e.g. pulsars, winds from massive stars, supernova remnants, solar flares, shocks in magnetic clouds, etc.), but the nature of the acceleration mechanism(s) in each source, and hence the predictability of its occurrence, remains unconfirmed. Single shock structures are not the only place where particle acceleration is thought to take place. In fact, large-scale shock–shock collisions, with their different hydrodynamic and kinetic structures, are also seen as potential sources of high-energy particles.

Super-critical shock collisions can be found in OB associations (very young stellar objects) (Higdon & Lingenfelter 2005; Ackermann *et al.* 2011; Rando & Buson 2015), consisting of many hot giant stars and characterized by supernova (SN) explosions that are correlated in space and time (Higdon, Lingenfelter & Ramaty 1998). In these objects, the strong winds of giant stars and of SN explosions contribute to generating large-scale structures that are known as 'superbubbles'. Inside these structures are vast amounts of mechanical, thermal and turbulent energy, making them appealing sources of cosmic rays. Among the many structures inside these superbubbles include super-critical shock–shock collisions: wind–wind, SN–wind and SN–SN shock collisions. The most common condition is the wind–wind shock collision in massive star binaries (Usov 1992; Sanchez-Bermudez *et al.* 2019), which is certainly a topic of large interest in astrophysics.

2. Former experimental results

2.1. *Single magnetized shock characterization*

In our former experiments performed at JLF/Titan and LULI2000 (Yao *et al.* 2021, 2022; Fazzini *et al.* 2022), we investigated single shock formation, as well as shock–shock interactions, by having an expanding plasma drive a shock into an ambient gas in the presence of a strong (20 T) external magnetic field. Since the expanding plasma, the ambient gas and the magnetic field are all decoupled, we are able to vary the magnetic field independently of the expanding plasma and of the ambient gas, which allows us to investigate the essential role played by the magnetic field and to highlight the ion acceleration mechanism at play.

With the set-up shown in figure 1(*a*), we have been able to characterize the plasma density, temperature, as well as the electric field developed at the front of a single shock, and observe strong non-thermal accelerated ion populations linked with the 'shock-surfing' acceleration mechanism (Yao *et al.* 2021, 2022).

Specifically, the shock was generated by sending a plasma, generated from a high-power laser (1 ns duration, 70 J, 1.6×10^{13} W cm^{-2}) irradiating a solid target (Teflon, or CF$_2$), into a low-density gas (of density $\sim 10^{18}$ cm^{-3}), and in the presence of a 20 T magnetic field that is homogeneous and steady state over the time scale of the experiment. This magnetic field is produced by our unique coil set-up (Albertazzi *et al.* 2013; Higginson *et al.* 2019). A record of the plasma electron density, obtained by optical probing, is shown in figure 1(*b*). We can clearly observe the presence of an electron foot, likely reflected ahead of the shock by the moving shock front. To our knowledge, this is the first laboratory observation of such a structure, which was postulated (Dimmock *et al.* 2019) and also verified to be present in magnetospheric shocks as recorded by satellite (Balogh & Treumann 2013).

Figure 1(*c*) shows the evolution of the shock front position and the corresponding velocity deduced from it, which shows the very fast decrease in shock velocity over the first few nanoseconds. Before 2.6 ns, the shock front velocity is approximately $v = 1500$ km s^{-1}, i.e. the shock is collisionless and super-critical with a mean free path
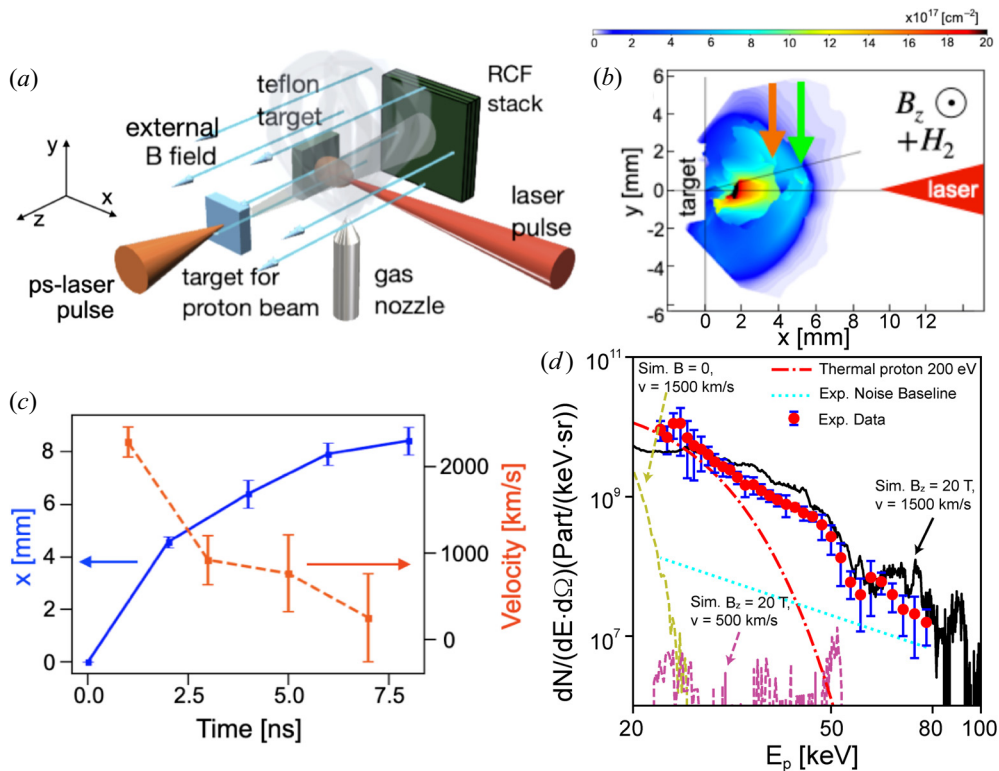
FIGURE 1. (*a*) Set-up of the experiment to characterize a single magnetized shock (Yao *et al.* 2021, 2022). The whole scene is embedded in an H_2 gas of low density ($\sim 10^{18}$ cm^{-3}) emanating from a pulsed nozzle. Further, the whole assembly is embedded in a strong magnetic field (20 T). (*b*) Density measurement (integrated along the line of sight) 4 ns after the laser irradiation of the solid target. (*c*) Evolution of the shock front position along the *x*-axis and the corresponding velocity. (*d*) Evidence for the energization of protons picked up from the ambient medium. Proton energy spectra of both the experiment (red dots) and of three PIC simulations, the black solid line for the magnetized fast case with applied magnetic field along the z-direction, i.e., $B_z = 20$ T and initial shock velocity $v = 1500$ km s^{-1}, the yellow dashed line for the unmagnetized fast one with $B = 0$ and $v = 1500$ km s^{-1}, and the purple dashed line for the magnetized slow one with $B_z = 20$ T and $v = 500$ km s^{-1}, all measured at t = 2.6 ns in the simulations. The analytical thermal proton spectrum is shown with the red dash-dotted line (200 eV); and the experimental noise baseline is shown in cyan dotted line.

larger than 10 mm and a magnetosonic Mach number larger than the critical value (see details in table 1), while after approximately 5 ns, it becomes sub-critical, with correspondingly lesser energization of the reflecting ions from the ambient (Yao *et al.* 2021, 2022). The ion spectrometer that was deployed in the experiment was set in the axis of the magnetic field, i.e. along the *z*-axis in figure 1(*a*), otherwise the ions energized out of the plasma could not be recorded, as they would be deflected away by the 20 T large-scale magnetic field.

The recorded proton spectrum is shown in figure 1(*d*) by red dots evidenced non-thermal proton energization. We have performed a series of particle-in-cell (PIC) simulations, using the code SMILEI (Derouillat *et al.* 2018), with different magnetic fields and initial shock velocities. Those simulations help us identify the critical role played by the external

	Plasma beta	M_{ms}	$\lambda_{mfp}/r_{L,i}$
Our Results	0.2	3.1	12.2
Earth's Bow Shock	0.4–0.8	2.8	1.2×10^8
Non-relativistic SNR	>1	20–100	10^4

TABLE 1. Comparison between the parameters of the shocks we are able to produce with our platform, and the ones of the solar wind, as well as those from a non-relativistic SNR (see Yao *et al.* 2021, p. 10). The parameters used for the calculations are: $B = 20$ T, $T_e = 100$ eV, $n_e = 3 \times 10^{18}$ cm^{-3}, $v_{shock} = 1500$ km s^{-1} (see details in text). The plasma beta is defined as $\beta \equiv P_{therm}/P_{mag}$ i.e. the ratio of plasma pressure to magnetic field pressure. The magnetosonic Mach number $M_{ms} = v_s/v_{ms}$, is the ratio between the shock velocity and the magnetosonic velocity ($v_{ms} \equiv \sqrt{v_A^2 + c_s^2}$) in the upstream medium, where v_A is the Alfvén velocity and c_s is the ion sound velocity. The fourth column allows one to evaluate that the shock is not affected by collisions. This requires that the ion–ion collision mean free path (λ_{mfp}) be large compared with the shocked-ion gyroradius, $r_{L,i}$, which sets the scale of the shock transition.

magnetic field and fast shock velocity in the non-thermal proton energization, i.e. only in the case with both 20 T magnetic field and 1500 km s^{-1} initial shock velocity can we well reproduce the experimental proton spectrum. Otherwise, the spectra will be lower than the noise baseline. Also note that there is no signal recorded above the noise baseline for cases with only the magnetic field or the ambient gas (i.e. when there will be no shock), indicating that the non-thermal particle populations are indeed coming from the shock.

The single shock front was also probed with protons in order to measure the electric field at that location (Yao *et al.* 2022). The probing protons accelerated by the Target Normal Sheath Acceleration (TNSA) (Mora 2003) were sent parallel to the magnetic field, as can be seen in figure 1(*a*). As shown in figure 2(*a*), we could clearly observe the same structure as in figure 1(*b*), namely the front of the expanding plasma and a particular proton deflection structure at the shock front. From it, as shown in figure 2(*b,c*), we can infer that the electric field at the shock front had a double jump structure, with a field reversal. Detailed discussions can be found in Yao *et al.* (2022).

The main parameters of the shock that we can produce with our set-up are summarized in table 1, showing that they are collisionless and super-critical, and actually quite close to those of the solar wind. Yet, reaching higher velocity shocks, with applicability to supernova remnants (SNR), is not possible with presently accessible high-power lasers, but will be in the near future with e.g. Apollon (Burdonov *et al.* 2021).

2.2. *Double magnetized shocks collision*

Later, we investigated at LULI2000, the interpenetration of two sub-critical single shocks with a similar set-up, which is shown in figure 3(*a*). Since the distance between the two targets was large (i.e. 9 mm), due to constraints in the set-up, the shocks travel to the middle and collide after 11 ns, as can be seen in figure 3(*c,d*), thus having an average velocity lower than 500 km s^{-1}. This led us to be limited to exploring sub-critical shock encounters (Fazzini *et al.* 2022).

The measured ion spectrum is the same as shown in figure 1(*d*). Nevertheless, our PIC simulations have revealed an interesting particle dynamics at play during the sub-critical shock encounter, and which provides energy enhancement (see figure 4). By tracking a set of representative energetic protons, we have indeed been able to identify that this
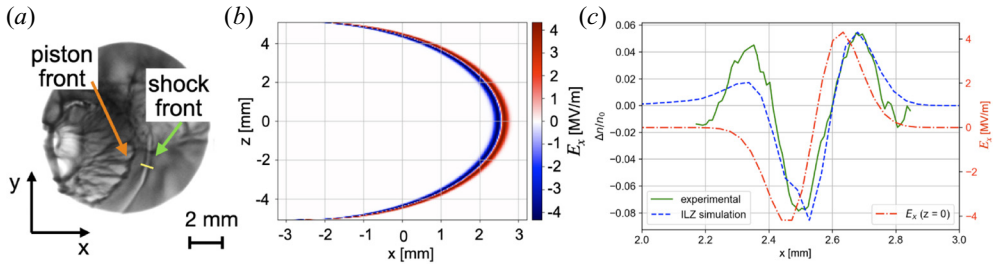
FIGURE 2. (*a*) Proton radiography (collected on a radiochromic film (RCF) and employing 19 MeV protons) of the same configuration as shown in figure 1(*a*), 5 ns after the laser pulse. (*b*) Hemispherical electric field E_x in the xz-plane, with a radius of $R = 5.1$ mm, estimated from (*a*). (*c*) Lineout of the proton dose modulation along the yellow line indicated in (*a*). The green full curve is the modulation from the experimental results, and the dashed blue curve is that from the ILZ simulation (Bolanos *et al.* 2022), which is obtained by imposing a bipolar electric field with hemispherical shape shown in (*b*). The red dash-dotted curve represents the lineout of the field E_x in $z = 0$ (Yao *et al.* 2022).
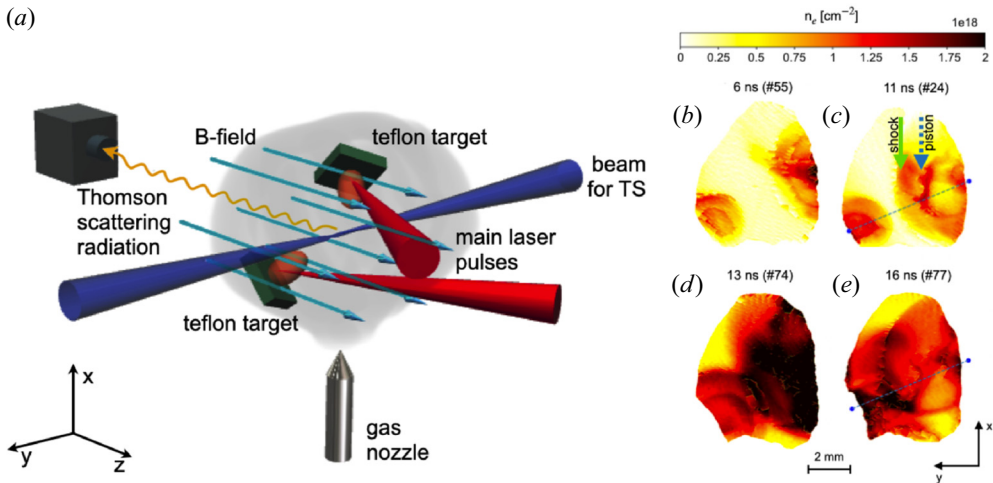

FIGURE 3. (*a*) Set-up of the experiment with two high-power lasers ((1 ns, 100 J at 1 μm wavelength, 1.6×10^{13} W cm^{-2} intensity on target)) irradiate two solid targets (CF$_2$) embedded in ambient gas and strong *B*-field (20 T). (*b–e*) Temporal sequence of the density (along the z-axis) measurements showing the evolution of the collision of two magnetized shocks.

energy enhancement is a result of the 'phase-locking effect' between the transverse particle velocity (V_y) and the transverse *E*-field (E_y) after the collision, i.e. the work done by E_y (i.e. W_{E_y}) is purely positive, which only exists in the shock colliding case and allows a further boost of the ion energy (Fazzini *et al.* 2022).

Unfortunately, the phase-locking effect could not be observed at LULI2000 since the time-integrated spectrum of ions is produced by a combination of ions accelerated by the super-critical shock early in time and the collision of the slowed-downed subcritical shock that would produce the phase-locking acceleration. Since, the maximum energy produced by these sub-critical shocks is low, we are not able to separate the two sources in our past measurements. This is why we propose to move, using an improved set-up, to investigate the encounter to the moments where the shocks are still super-critical.
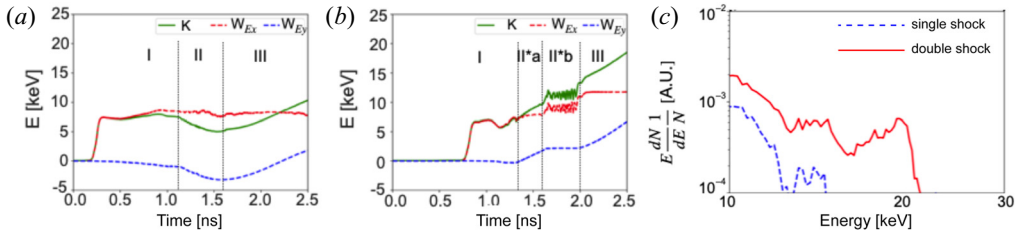
FIGURE 4. The PIC simulation results demonstrating the enhanced particle acceleration in the sub-critical shock colliding case (*b*), compared with the single one (*a*). The final energy spectrum is in (*c*). See details of the three phases in Fazzini *et al.* (2022).

3. Future plans

As shown above, in our previous work investigating the collision of two sub-critical shocks, we have revealed an interesting effect of phase locking of the ions trapped between the two counter-streaming shocks, resulting in boosts to their energy. We have now performed PIC simulations to gauge how this effect would manifest in encountering super-critical shocks.

The set-up of the simulation is the same as our former works, see details in figure 9 of Fazzini *et al.* (2022). Only here the initial drift velocity becomes $1500 \, \text{km} \, \text{s}^{-1}$, which can be realized in the experiment by putting the two targets closer to each other, e.g. 4 mm.

Figure 5(*a,b*) shows the time evolution of the energy of ions, as well as the contribution from the longitudinal (W_{Ex}) and transverse (W_{Ey}) electric fields (the energy that they pick up while gyrating in the field) in the case of both a single and of colliding shocks. One can observe that there is, in the colliding case, the same phase-locking effect (i.e. W_{Ey} stays positive due to the shock collision), which induces a significant particle acceleration enhancement. This is shown in the final ion energy spectrum plotted in figure 5(*c*). Based on our previous experience in measuring ions energized by single super-critical shocks (Yao *et al.* 2021, 2022), this further and strong energization should be easily detectable and recognizable.

This experiment is programmed to be performed at RAL-TAW in 2023, due to its unique multi-beam capability to generate two super-critical shocks (using two long pulse beams), and we will characterize them in detail using optical probing, proton radiography (powered by using the facility high-energy short-pulse B8 beam), space-resolved X-ray spectroscopy and Thomson scattering. We will lift the limitation that was preventing us at LULI2000 (due to a constraint in the laser beam arrangement) to investigate super-critical shock encounters by having a closer arrangement of the targets, thus ensuring the shocks meet before 5 ns in their evolution. Figure 6 shows the proposed set-up in the horizontal plane. The two targets, from which the two shocks will be launched, will directly face each other, which will also allow for a straight, face-on collision of the shocks. Long f-number long pulses (in yellow) will irradiate each target and induce the plasma expansion. A pulsed gas jet (coming from the bottom of the coil) will provide the ambient plasma; the gas is ionized by the X-rays from the laser–target interaction. As shown in figure 6(*a*), the short pulse will be focused on a solid target at the edge of the coil. A TNSA-accelerated proton beam will emerge from the target back side and diagnose the shocks and field structures on an RCF stack. Alternatively to this proton radiography diagnostic, we will set, along the axis of the magnetic field, a time-of-flight (ToF) spectrometer which will measure the time at which ions land on a photomultiplier tube (PMT) (Fourmaux *et al.* 2013), as shown
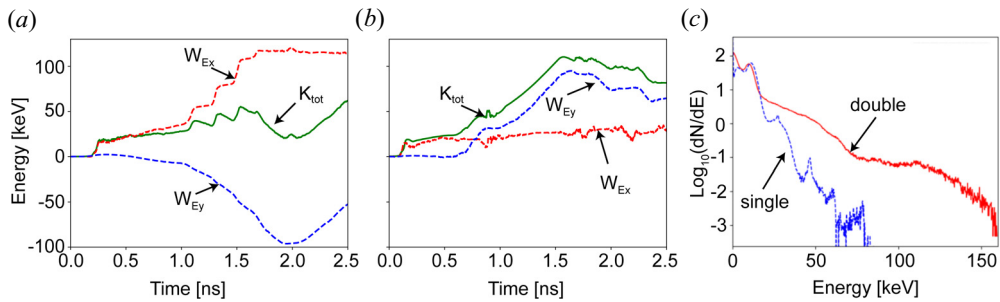
FIGURE 5. The PIC simulation results demonstrating the enhanced particle acceleration in the super-critical shock colliding case (*b*) we propose to investigate, compared with the single shock one (*a*), with an initial drift velocity of $1500 \, \mathrm{km \, s^{-1}}$ under a 20 T magnetic field. The final energy spectrum is in (*c*), showing an enhancement of the maximum energy by a factor 2 for the colliding shocks case. Note that now the energy spectrum of the colliding case can be observed in the experiment, since it is higher than that of the ions accelerated in the single shock, i.e. reaching around 80 keV, see figure 1(*d*).
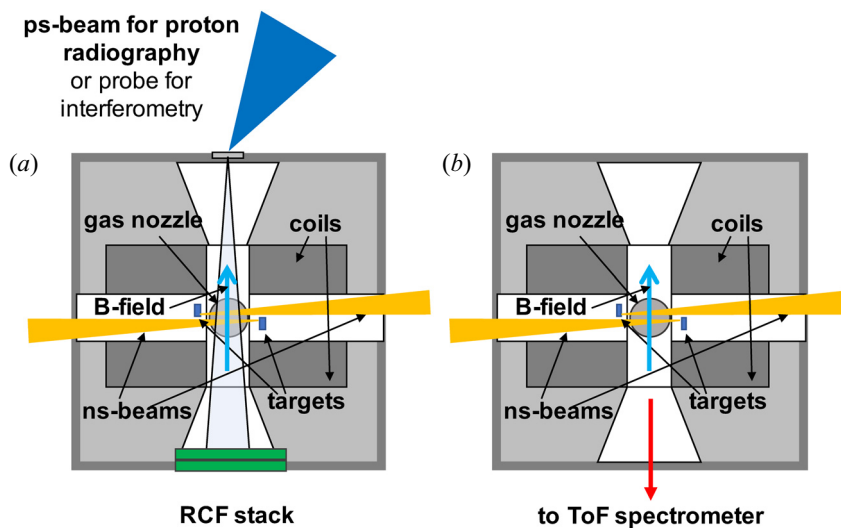
FIGURE 6. Detailed view inside the coil of the proposed set-up. The two ns-laser beams hit the two targets, giving rise to two face-on collisionless shocks, embedded in the 20 T *B*-field and a $10^{18} \, \mathrm{cm^{-3}}$ ambient gas, that meet at the centre of the coil. In set-up (*a*), proton radiography or optical probing will be used along the main *B*-field axis to diagnose the colliding shocks. Alternatively, in set-up (*b*), a ToF spectrometer will be used, also along the *B*-field axis, to diagnose the dynamics of particle acceleration taking place in the plasma.

in figure 6(*b*). From it, we will be able to observe the dynamics and the energy of particle acceleration induced within the plasma.

4. Conclusion

In summary, by re-using the platform we established at LULI2000 and JLF/TITAN to investigate the dynamics of magnetized shocks and the associated particle acceleration, our future plan will focus on characterizing experimentally the particle acceleration

enhancement during the collision of two super-critical shocks. It will serve as the direct proof of our theoretical analysis, possibly confirming the phase-locking effect induced by the shock collisions (Fazzini *et al.* 2022) for the first time in the laboratory.

Acknowledgements

Funding

Declaration of interests

The authors report no conflict of interest.

Author contributions statement

J.F. conceived the project. A.F., S.N.C., K.B. and J.F. performed the experiments. W.Y., A.F., K.B. and J.F. analysed the data. W.Y. performed and analysed the SMILEI simulations with discussions with A.C., X.R., E.d.H. and J.F. W.Y. wrote the bulk of the paper, with major contributions from S.N.C., M.B., M.M., S.O. and J.F. All authors commented and revised the paper.

Data availability statement

All data needed to evaluate the conclusions in the paper are present in the paper. Experimental data and simulations are archived on servers at LULI laboratory and are available from the corresponding author upon reasonable request.

REFERENCES

ACKERMANN, M., AJELLO, M., ALLAFORT, A., BALDINI, L., BALLET, J., BARBIELLINI, G., BASTIERI, D., BELFIORE, A., BELLAZZINI, R., BERENJI, B., *et al.* 2011 A cocoon of freshly accelerated cosmic rays detected by fermi in the cygnus superbubble. *Science* **334** (6059), 1103–1107.

ALBERTAZZI, B., BÉARD, J., CIARDI, A., VINCI, T., ALBRECHT, J., BILLETTE, J., BURRIS-MOG, T., CHEN, S.N., DA SILVA, D., DITTRICH, S., *et al.* 2013 Production of large volume, strongly magnetized laser-produced plasmas by use of pulsed external magnetic fields. *Rev. Sci. Instrum.* **84** (4), 043505.

BALOGH, A. & TREUMANN, R.A. 2013 *Physics of Collisionless Shocks: Space Plasma Shock Waves*. Springer Science & Business Media.

BOLANOS, S., SMETS, R., CHEN, S.N., GRISOLET, A., FILIPPOV, E., HENARES, J.L., NASTASA, V., PIKUZ, S., RIQUIER, R., SAFRANOVA, M., *et al.* 2022 Laboratory evidence of magnetic reconnection hampered in obliquely interacting flux tubes. *Nat. Commun.* **13** (1), 1–12.

BURDONOV, K., FAZZINI, A., LELASSEUX, V., ALBRECHT, J., ANTICI, P., AYOUL, Y., BELUZE, A., CAVANNA, D., CECCOTTI, T., CHABANIS, M., *et al.* 2021 Characterization and performance of the Apollon short-focal-area facility following its commissioning at 1 PW level. *Matter Radiat. Extrem.* **6** (6), 064402.

DEROUILLAT, J., BECK, A., PÉREZ, F., VINCI, T., CHIARAMELLO, M., GRASSI, A., FLÉ, M., BOUCHARD, G., PLOTNIKOV, I., AUNAI, N., *et al.* 2018 SMILEI: a collaborative, open-source, multi-purpose particle-in-cell code for plasma simulation. *Comput. Phys. Commun.* **222**, 351–373.

DIMMOCK, A.P., RUSSELL, C.T., SAGDEEV, R.Z., KRASNOSELSKIKH, V., WALKER, S.N., CARR, C., DANDOURAS, I., ESCOUBET, C.P., GANUSHKINA, N., GEDALIN, M., *et al.* 2019 Direct evidence of nonstationary collisionless shocks in space plasmas. *Sci. Adv.* **5** (2), eaau9926.

FAZZINI, A., YAO, W., BURDONOV, K., BÉARD, J., CHEN, S.N., CIARDI, A., D'HUMIÈRES, E., DIAB, R., FILIPPOV, E.D., KISYOV, S., *et al.* 2022 Particle energization in colliding subcritical collisionless shocks investigated in the laboratory. *Astron. Astrophys.* **665**, A87.

FOURMAUX, S., BUFFECHOUX, S., ALBERTAZZI, B., CAPELLI, D., LÉVY, A., GNEDYUK, S., LECHERBOURG, L., LASSONDE, P., PAYEUR, S., ANTICI, P., *et al.* 2013 Investigation of laser-driven proton acceleration using ultra-short, ultra-intense laser pulses. *Phys. Plasmas* **20** (1), 013110.

HIGDON, J.C. & LINGENFELTER, R.E. 2005 OB associations, supernova-generated superbubbles, and the source of cosmic rays. *Astrophys. J.* **628** (2), 738.

HIGDON, J.C., LINGENFELTER, R.E. & RAMATY, R. 1998 Cosmic-ray acceleration from supernova ejecta in superbubbles. *Astrophys. J.* **509** (1), L33.

HIGGINSON, D.P., KORNEEV, P., RUYER, C., RIQUIER, R., MORENO, Q., BÉARD, J., CHEN, S.N., GRASSI, A., GRECH, M., GREMILLET, L., *et al.* 2019 Laboratory investigation of particle acceleration and magnetic field compression in collisionless colliding fast plasma flows. *Commun. Phys.* **2** (1), 1–7.

MORA, P. 2003 Plasma expansion into a vacuum. *Phys. Rev. Lett.* **90** (18), 185002.

RANDO, R. & BUSON, S. 2015 Fermi LAT: more than six years of insights and new puzzles. *La Rivista del Nuovo Cimento* **38** (5), 209–269.

SANCHEZ-BERMUDEZ, J., ALBERDI, A., SCHÖDEL, R., BRANDNER, W., GALVÁN-MADRID, R., GUIRADO, J.C., HERRERO-ILLANA, R., HUMMEL, C.A., MARCAIDE, J.M. & PÉREZ-TORRES, M.A. 2019 A VLBI study of the wind-wind collision region in the massive multiple HD 167971. *Astron. Astrophys.* **624**, A55.

USOV, V.V. 1992 Stellar wind collision and x-ray generation in massive binaries. *Astrophys. J.* **389**, 635–648.

YAO, W., FAZZINI, A., CHEN, S.N., BURDONOV, K., ANTICI, P., BÉARD, J., BOLAÑOS, S., CIARDI, A., DIAB, R., FILIPPOV, E.D., *et al.* 2022 Detailed characterization of a laboratory magnetized supercritical collisionless shock and of the associated proton energization. *Matter Radiat. Extrem.* **7** (1), 014402.

YAO, W., FAZZINI, A., CHEN, S.N., BURDONOV, K., ANTICI, P., BÉARD, J., BOLAÑOS, S., CIARDI, A., DIAB, R., FILIPPOV, E.D., *et al.* 2021 Laboratory evidence for proton energization by collisionless shock surfing. *Nat. Phys.* **17** (10), 1177–1182.